

# Four-User, 2.5-Gb/s, Spectrally Coded OCDMA System Demonstration Using Low-Power Nonlinear Processing

Z. Jiang, *Student Member, IEEE*, D. S. Seo, *Member, IEEE*, S.-D. Yang, *Student Member, IEEE*, D. E. Leaird, *Member, IEEE*, R. V. Roussev, C. Langrock, *Student Member, IEEE*, M. M. Fejer, and A. M. Weiner, *Fellow, IEEE, Fellow, OSA*

**Abstract**—This paper describes the demonstration of 2.5-Gb/s four-user optical-code-division-multiple-access (OCDMA) system operating at bit-error rate  $\leq 10^{-11}$  utilizing programmable spectral phase encoding, an ultrasensitive ( $\sim 200$  fJ/b) periodically poled lithium-niobate-waveguide nonlinear waveform discriminator and 10G Ethernet receiver. A comprehensive description of this ultra-short-pulse spectral phase-coded OCDMA system is presented. On the subsystem level, two key component technologies, namely, femtosecond encoding/decoding and low-power high-contrast nonlinear discrimination, have been developed and characterized. At the system level, data for the four-user OCDMA system operating at 2.5 Gb/s for binary as well as multilevel code families are described.

**Index Terms**—Multiaccess interference (MAI), nonlinear optics, optical code-division multiple access (OCDMA), optical signal processing, pulse shaping.

## I. INTRODUCTION

MULTIPLE-ACCESS techniques are required to meet the demand for high-speed, large-capacity communications in optical networks, which allow multiple users to share the fiber bandwidth. There are three major multiple access approaches. Each user is allocated a specific time slot in time-division multiplexing (TDM) and a specific frequency (wavelength) slot in wavelength-division multiplexing (WDM). Both techniques have been extensively explored and utilized in optical communication systems [1]–[6]. Alternatively, optical-code-division multiple access (OCDMA) [7]–[34], [62] is receiving increasing attention due to its potential for enhanced information security, simplified and decentralized network control, improved spectral efficiency, and increased flexibility

in the granularity of bandwidth that can be provisioned. In OCDMA, different users whose signals may be overlapped both in time and frequency share a common communications medium; multiple access is achieved by assigning different, minimally interfering code sequences to different code-division multiple-access (CDMA) transmitters, which must subsequently be detected in the presence of multiaccess interference (MAI) from other users. Fig. 1 shows a schematic illustration of bandwidth allocation in TDM, WDM and OCDMA.

CDMA derives from radio-frequency (RF) spread-spectrum communications, originally developed for military applications due to an inherent low probability of intercept and immunity to interference, and more recently for commercial RF cellular radio applications [35], [36]. CDMA is now becoming the dominant multiple-access technique in RF wireless networks. Since RF-CDMA works with typical carrier frequencies in the  $\sim 1$ -GHz range and bit rates on the order of  $\sim 100$  kb/s, current electronic technologies can easily provide coding and long temporal codes ( $\sim 1000$  chips) for each bit, which is critical to support a large number of potential users [7]. In addition, the bit-error-rate (BER) requirement is usually not so strict for RF-CDMA. In contrast, the need to perform encoding and decoding for OCDMA poses one immediate challenge because of both the optical carrier frequency and the much higher bit rate of  $\sim$ Gb/s per user, which already approaches the limit of electronic processing. Therefore, innovative all-optical processing technologies are needed. In addition, the challenges for OCDMA also come from critical requirements that are routinely required in optical communication systems. These requirements include extreme high quality of service (QoS) (BER at  $10^{-9}$  or below), large capacity (tens or hundreds of users, total capacity up to  $\sim 100$  Gb/s or above), and long distance [kilometers to  $\sim 100$  km for local area networks (LANs) and metropolitan area networks (MANs)].

Several different OCDMA schemes have been proposed [8]–[34], [62], based on different choices of sources, coding schemes, and detection. OCDMA schemes may be classified according to the choice of coherent versus incoherent processing, coherent (mode-locked pulses) versus incoherent [e.g., amplified spontaneous emission (ASE) and light-emitting diode (LED)] broad-band optical source, and encoding method (time-domain versus frequency-domain, amplitude versus phase). Schemes based on incoherent processing (summing of optical powers) and broad-band incoherent (noise) sources

Manuscript received May 19, 2004; revised October 12, 2004. This work supported in part by the Defense Advanced Research Projects Agency (DARPA) under Grant MDA972-03-1-0014 and by the U.S. Air Force under Grant F49620-02-1-0240. The work of D. S. Seo was supported in part by the Korea Science and Engineering Foundation (KOSEF) under Grant R01-2003-000-10444-0 and by Inha University, Engineering Research Center (ERC), Korea.

Z. Jiang, S.-D. Yang, D. E. Leaird, and A. M. Weiner are with the School of Electrical and Computer Engineering, Purdue University, West Lafayette, IN 47907-2035 USA (e-mail: zjiang@purdue.edu).

D. S. Seo is with the School of Electrical and Computer Engineering, Purdue University, West Lafayette, IN 47907-2035, USA, on leave from the Department of Electronics, Myongji University, Yongin 449-728, Korea.

R. V. Roussev, C. Langrock, and M. M. Fejer are with the Edward L. Ginzton Laboratory, Stanford University, Stanford, CA 94305-4088 USA.

Digital Object Identifier 10.1109/JLT.2004.840039

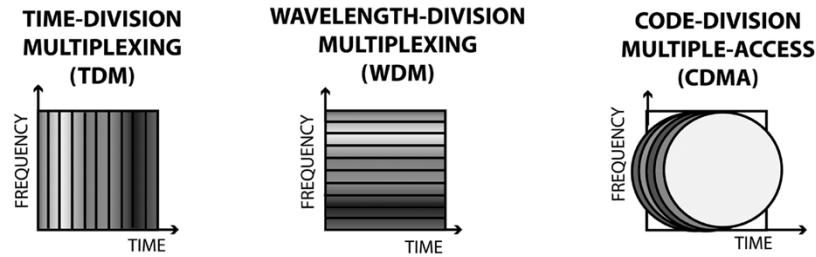


Fig. 1. Schematic illustration of bandwidth allocation in TDM, WDM, and CDMA optical networks.

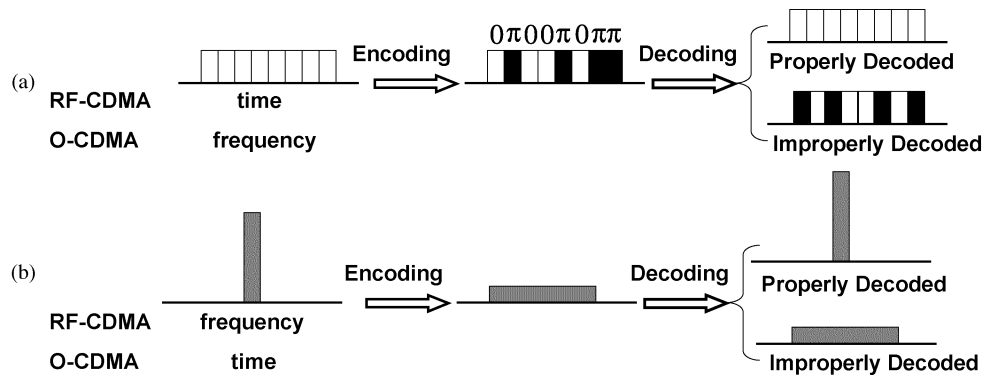


Fig. 2. Comparison of DS RF-CDMA and spectral-phase-coded OCDMA. (a) Time-domain behavior for RF-CDMA (equivalent to frequency-domain behavior for OCDMA). (b) Frequency-domain behavior for RF-CDMA (equivalent to time-domain behavior for O-CDMA).

are generally the easiest to implement but offer relatively poor performance. To increase the available coding space, time-wavelength (two-dimensional, or 2-D) coding schemes have been proposed, where each code chip corresponds to a specific time position and wavelength position within a bit as determined by a code matrix [22], [30], [31]. This scheme may utilize either coherent or incoherent sources but employs incoherent processing (summing of optical powers from chips with different wavelength and time positions). However, as in radio spread-spectrum systems, coherent processing based on manipulation of optical fields, which can be made to sum to zero, is needed for strongest suppression of MAI and for best performance. Here, an ultra-short-pulse OCDMA scheme based on spectral phase encoding and decoding of coherent mode-locked pulses [10], [15] is experimentally investigated. A theoretical analysis of the MAI-limited performance of this approach indicates the potential for OCDMA systems with capacities from tens to perhaps  $\sim 100$  Gb/s in fully asynchronous operation, depending on how short a pulsewidth and how long a code length can be implemented in the system [10].

The proposed ultra-short-pulse OCDMA scheme based on spectral phase encoding has an interesting analogy with the most widely used direct sequence (DS) RF-CDMA. Fig. 2 shows time- and frequency-domain evolution during encoding/decoding for these two schemes. For DS RF-CDMA, a bit is divided into many temporal chips and phase-coded for each chip [for example, 0 or  $\pi$  phase shift for bipolar phase shift keying (BPSK)] in the time domain [Fig. 2(a)] so that the spectrum of a narrow-band signal is broadened during the encoding process [Fig. 2(b)]. After decoding at the receiver, a properly decoded signal is recovered back to a narrow-band signal, which can be separated out by a narrow-band filter from

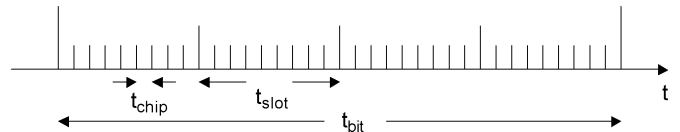


Fig. 3. Timing control in OCDMA optical networks.

the improperly decoded broad-band MAI. This encoding/decoding process manifests the spread-spectrum property of DS RF-CDMA [35], [36] where there exists a tradeoff between bandwidth and performance. The proposed OCDMA scheme is just a time-frequency-reversed version of DS RF-CDMA, where the ultra-short-pulse spectrum is divided to many frequency chips and phase-coded for each chip [Fig. 2(a)]. This results in spreading in the time domain [Fig. 2(b)], while proper decoding “de-spreads” the encoded signal back to its original duration in time.

CDMA is well suited for bursty network environments, and the asynchronous nature of data transmission can simplify and decentralize network management and control. However, due to system requirements mentioned previously, full asynchronism is difficult to implement in practice while simultaneously maintaining sufficient MAI suppression. Therefore, some level of synchronism is built into many  $\geq$ two-user OCDMA schemes. The time scales relevant for a discussion of synchronism requirements are illustrated in Fig. 3. The coarsest time scale is the bit period  $t_{bit}$ . Uncoded or properly decoded waveforms have a duration that is called the chip duration  $t_{chip}$ . Encoded or improperly decoded pulses are pseudonoise waveforms with a larger duration, which is referred to here as the slot duration  $t_{slot}$ . In the proposed spectral-phase-coded OCDMA scheme, the individual features in the pseudonoise

TABLE I  
COMPARISON OF OCDMA SCHEMES IN TERMS OF TIMING REQUIREMENT

Receiver requirement \ Transmitter requirement	No coordination	Slot level coordination	Chip level coordination
Asynchronous detection (via nonlinear optical processing)	TR: low Ref: [16]	TR: medium Ref: this work	TR: high Ref: [33]
Synchronous detection requiring chip level ( $t_{\text{chip}}$ ) speed (either electronically or via optical gating with clock recovery)	TR: high Ref: [22,27]	TR: high Ref: -	TR: high Ref: [19,20,21,32]

TR: timing requirement, Ref: references. Not all the references include a sufficiently detailed timing discussion. For references [19], [22], [27], detection was clearly based on gating with chip-level synchronism; however, the level of timing coordination at the transmitter was not clearly specified. In those cases the classification was made according to the authors' best interpretation.

waveforms have characteristic durations equal to  $t_{\text{chip}}$ , and the number of independent features is equal to the code length  $N$ , i.e.,  $t_{\text{slot}}/t_{\text{chip}} = N$ . For a fully asynchronous system, signals transmitted by any user can fall anywhere within a bit duration  $t_{\text{bit}}$  without coordination with other users. In a fully synchronous system, the signal transmitted by any specific user must be coordinated with the transmission time of all the other users, with a timing precision below  $t_{\text{chip}}$ . Furthermore, a synchronous receiver would require optical clock recovery for gating with timing precision also below  $t_{\text{chip}}$ . To relax the timing requirements of the fully synchronous approach, the authors of the present paper propose the concept of slot-level coordination—the transmission time of a user is controlled on the time scale of the slot duration  $t_{\text{slot}}$  but without the need for chip-level timing control. Accordingly, OCDMA can be classified according to different levels of synchronism requirements. At the transmitter side, there are distinctions between no coordination (full asynchronism) versus slot-level ( $t_{\text{slot}}$ ) coordination versus chip-level ( $t_{\text{chip}}$ ) coordination. At the receiver side, there are distinctions between asynchronous detection versus synchronous detection requiring chip-level ( $t_{\text{chip}}$ ) speed (either electronically or via optical gating with clock recovery). All the possible combinations are listed in Table I with representative references. It is clear that chip-level transmission coordination and/or synchronous detection requiring chip-level ( $t_{\text{chip}}$ ) speed are used in many  $\geq$ two-user OCDMA schemes. This sacrifices one of the most significant advantages, asynchronism, of CDMA. In contrast, the proposed scheme only requires slot-level coordination, and fully asynchronous detection is achieved by means of a novel asynchronous nonlinear optical processing technique.

Fig. 4 shows the conceptual OCDMA network diagram for many of the OCDMA approaches. Input ultra-short pulses are time-spread during the encoding process into lower intensity noise-like signals [15]–[34], [62]. In the receiver, data corresponding to a desired user is separated from MAI via a matched filtering (decoding) operation, in which properly decoded signals are converted back to the original pulselike signals, while improperly decoded signals remain low-intensity, noise-like,

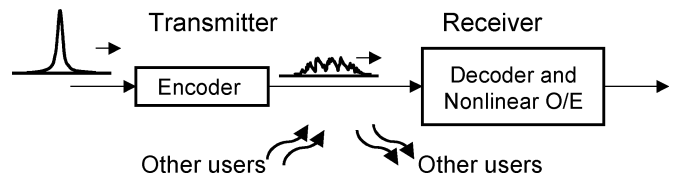


Fig. 4. Conceptual diagram of an OCDMA network.

temporally broad waveforms. Since the energy in properly and improperly decoded signals remains similar, and since the temporal duration of even improperly decoded signals is on the order of the bit period or below, both properly and improperly decoded signals will appear essentially identical to an electronic receiver band-limited to the data rate. Consequently, either very fast electronics or a nonlinear optical intensity discriminator play a critical role in separating properly decoded short pulses from improperly decoded MAI.

In previous literature, interference rejection was achieved using a nonlinear fiber-optic discriminator in a fully asynchronous two-user experiment using spectral phase encoding/decoding but operated at only  $\sim 50$  Mb/s [15]–[17]. An AWG-based device has been used for encoding/decoding of a single 10-Gb/s data stream; however, the crucial interference rejection function was not demonstrated [18]. Fiber grating encoders have been used to demonstrate two simultaneous frequency-overlapped 1.25-Gb/s users using fast electronics for waveform discrimination [26]. Fiber gratings were also used in a single-user 1.25-Gb/s experiment using a nonlinear fiber device for contrast enhancement; however, no testing with multiuser interference was reported [25]. An OCDMA/WDM/TDM overlay experiment demonstrated very high aggregate bit rates but relied on synchronous nonlinear gating in the receiver, with timing coordination and synchronism required down to  $\sim 1$  ps [20], [21]. Recently a four-user 1.25-Gb/s system has been demonstrated using spectral phase coding and a highly nonlinear fiber for MAI suppression [33]. This experiment required coordination of transmitted signals with chip-level timing requirements as well as relatively high powers at the receiver.

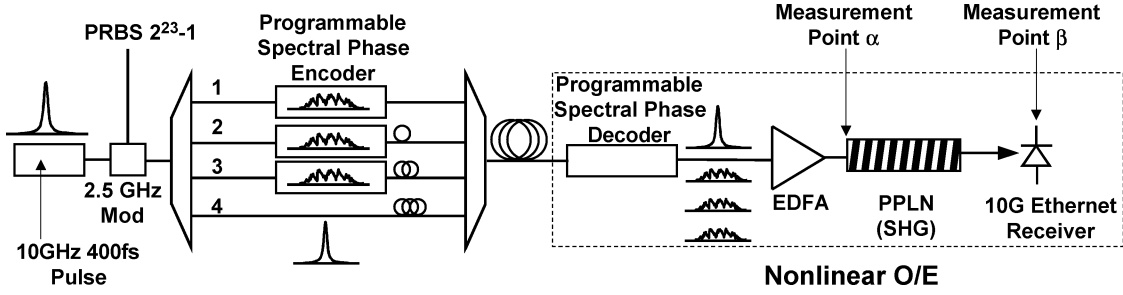


Fig. 5. Four user OCDMA system testbed.

This paper describes the demonstration of a four-user spectral-phase-coded OCDMA system operating at 2.5 Gb/s with strong nonlinear interference suppression. Compared with previous literature, there are two key points, as follows: 1) full interference suppression with four users at gigabit-per-second rates without the need for chip-level timing coordination or synchronous gating and 2) the use of a novel ultrasensitive nonlinear optical intensity discriminator based on second harmonic generation (SHG) in a periodically poled lithium niobate (PPLN) waveguide. The nonlinear discriminator used permits full MAI suppression at an operating energy of  $\sim 200$  fJ/bit, as much as two orders of magnitude lower than previous discriminators based on nonlinear fiber optics [15], [16], [20], [21], [25], [33]. The ability to operate at low power per user is critical for scaling an OCDMA system to multiple users.

The power scaling issue can be understood as follows. Let us assume that the self-gated nonlinear discriminator key to the proposed scheme requires some value  $U_{\text{bit}}$  to achieve a desired BER performance, where  $U_{\text{bit}}$  is the energy required per bit for a single properly decoded user. Since equal samples of each channel are seen by every OCDMA receiver, the average power required at the nonlinear element is  $0.5 CB U_{\text{bit}}$ , where  $C$  is the number of channels,  $B$  is the data rate, and the factor 0.5 comes from ON-OFF keying (OOK). Previous demonstrations of OCDMA nonlinear discriminators were based on nonlinear fiber optics, where typical values for  $U_{\text{bit}}$  range from 5–50 pJ [15], [25]. For four 2.5-Gb/s channels, this gives an average power requirement of 14–24 dBm at each receiver. Scaling to significantly higher bit rates and channel numbers would require a very large optical amplifier at each receiver, which is highly undesirable for application to networks with large numbers of nodes. To address this scaling issue, it is critical to reduce  $U_{\text{bit}}$ . The experiments using waveguide SHG generation achieve  $\sim 200$  fJ/bit at 2.5 Gb/s, a reduction approaching two orders of magnitude compared with discriminators based on nonlinear fiber optics.

It is noted that very recently, subsequent to the submission of this paper, four-user 10-Gb/s spectral-phase-coded OCDMA system experiments have been reported both by the authors of the present paper and by another group. These references are included for completeness [60], [61].

The remainder of this paper is structured as follows. In Section II, the ultra-short-pulse spectral-phase-coded OCDMA testbed and key enabling components are described. Section III presents the four-user system experiment with all of the OCDMA subsystems connected together. In Section IV,

some challenges for ultra-short-pulse OCDMA implementation as revealed by the experiments are discussed, and Section V concludes the paper.

## II. OCDMA SYSTEM AND COMPONENTS

A schematic diagram of the four user OCDMA demonstration is shown in Fig. 5. An actively mode-locked fiber laser followed by a dispersion-decreasing fiber (DDF) soliton compressor producing nearly transform-limited 400-fs pulses at 10 GHz centered near 1542 nm is used as the pulse source. A 2.5-Gb/s pseudorandom bit sequence (PRBS)  $2^{23} - 1$  data stream is impressed on the laser output (four pulses in each bit) with an intensity modulator, and then a  $1 \times 4$  passive splitter is used to generate the four separate users. For three of the users, the data-modulated ultra-short pulses are input into encoders constructed from fiber-coupled Fourier transform pulse shapers [38]–[40] to spectrally phase code the spectrum of the source laser. A fourth uncoded user path is also present to serve as an additional strong interference channel. Since this uncoded path shows essentially the same noiselike characteristics as other users after it is improperly decoded, this is sufficient to evaluate MAI effects. All four users are independently controlled to equalize their powers and to obtain identical polarizations at the receiver in order to correctly evaluate the effect of MAI. The output data from each user path are decorrelated by a fiber delay line and then combined to a short transmission fiber. Appropriate lengths of dispersion-compensating fiber (DCF) are used to compensate the dispersion of the user paths. Only single-mode fiber (SMF) and DCF are used in our experiments; polarization-maintaining (PM) fiber is not employed. The receiver consists of another fiber-coupled Fourier transform pulse shaper which selects (decodes) the desired user channel, an optical amplifier, a highly sensitive fiber-pigtailed PPLN waveguide chip to perform the nonlinear discrimination function, and a 2.4-GHz bandwidth photoreceiver, adapted from 10-Gb/s Ethernet, operating at the second harmonic wavelength of  $0.77 \mu\text{m}$ . The detailed descriptions of the key enabling components are as follows.

### A. 10-GHz 400-fs Pulse Source

A home-made actively mode-locked fiber laser [37] is used which allows center wavelength tuning from 1535 to 1560 nm and repetition rate tuning from 8 to 13 GHz, while keeping a  $2.5 \sim 3.5$  ps (full-width-at-half-maximum, or FWHM) short pulse. In the current paper, the center wavelength is 1542 nm, and the repetition rate is 9.9988 GHz, generating a 2.6-ps pulse.

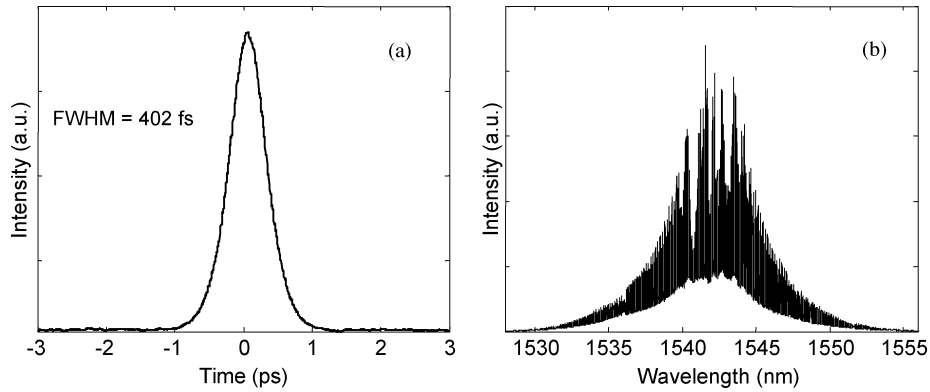


Fig. 6. 10-GHz 400-fs pulse: (a) intensity autocorrelation measurement and (b) optical spectrum.

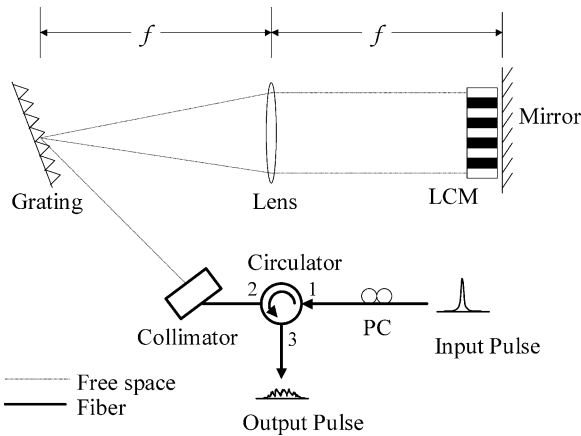


Fig. 7. Reflective pulse shaper used as encoder/decoder.  $f$ : Focal length, PC: Polarization controller. LCM: Liquid-crystal modulator.

In order to achieve sufficient bandwidth for OCDMA spectral phase coding, the laser output is followed by a DDF soliton compressor to produce nearly transform-limited  $\sim 400$ -fs pulses assuming hyperbolic secant pulse shape. An intensity autocorrelation measurement of the pulses after the DDF and the optical spectrum are shown in Fig. 6.

### B. Pulse Shaper Encoder/Decoder

Both encoding and decoding are implemented by the well-developed ultra-short-pulse shaping techniques [38]–[40] using a fiber-coupled Fourier transform pulse shaper which incorporates a 128-element liquid-crystal modulator (LCM) array to spectrally phase code the spectrum of the source laser. The individual pixels of the LCM can be electronically controlled independently to give an arbitrary phase shift in the range of 0 to  $2\pi$  with 12-bit resolution. Fig. 7 shows the reflective pulse shaper configuration used in our experiment [41]. Since the diffraction grating in our setup is polarization dependent, a polarization controller (PC) is used before circulator port 1. A collimator is connected to circulator port 2. A telescope could be inserted after the collimator to magnify the beam size on the grating in order to enhance the spectral resolution. Discrete frequency components making up the input short pulse are horizontally diffracted by the grating and focused by the lens at the retro-reflecting mirror. The LCM is placed just before the lens focal plane to enable programmable spectral phase coding. A retro-

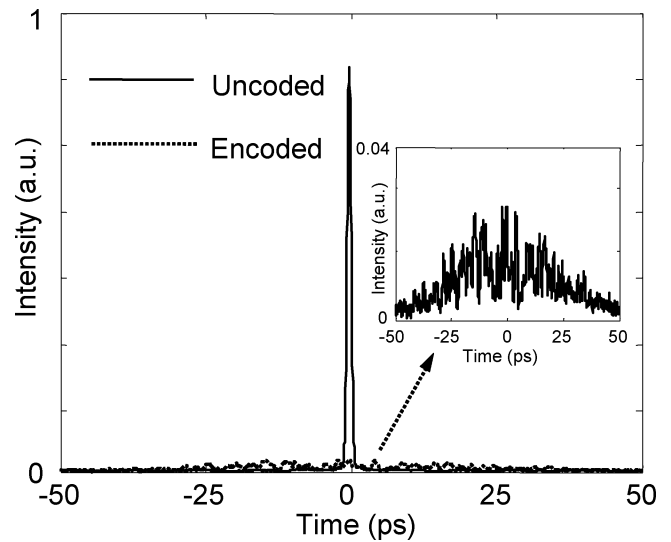


Fig. 8. Intensity cross-correlation measurements of uncoded (solid line) and 127 MS encoded (dotted line) pulses. Inset figure shows encoded pulse with enhanced vertical scale.

reflecting mirror leads to a double pass geometry, with all the frequencies recombined into a single fiber and with the output from circulator port 3. The pulse shaper is easily programmed under computer control, which allows convenient testing of various code families.

In order to optimize system performance, we investigated several pulse shaper designs for use in OCDMA. In general, high spectral resolution and low loss are the most critical issues in the designs. Unfortunately, there exists a tradeoff between high resolution and low loss in our current designs. More code chips for spectral phase coding can be achieved in a high-resolution pulse shaper, which is critical to scale to a large number of users in OCDMA implementations [10]. The resolution here is defined as the beam diameter (intensity decreases to  $1/e^2$  of peak value) at the LCM plane for each single frequency component. Since 128 pixels of the LCM cover 12.8 mm, each with  $\sim 100$ - $\mu\text{m}$  active width, a maximum of 128 coded chips is feasible if the resolution is equal to or less than  $100 \mu\text{m}$ . Fig. 8 shows intensity cross-correlation measurements of uncoded and encoded pulses with such a high-resolution shaper. The uncoded (LCM set for all pixels at zero phase) pulse is quite similar to the input 400-fs pulse, which is characteristic of a

TABLE II  
REFLECTIVE PULSE SHAPER PARAMETERS

	High resolution Pulse shaper	Encoder for User 1 (low loss)	Encoder for User 2	Encoder for User 3	Decoder
Collimator beam diameter (mm) *	5.4	1.9	2.7	5.4	2.7
Grating lines (/mm)	1100	1100	1100	860	1100
Grating diffraction angle (degree)	49	52	52	53	52
lens focal length (mm)	500	400	400	500	400
Spectral coding Range at the LCM $\Delta\lambda$ (nm)	15.3	17.9	17.9	17.9	17.9
Resolution ** ( $\mu\text{m}$ )	100	300	200	260	200
Supported chip count	128	42	64	42	64
Loss (dB)	8.5	4.0	4.5	8.5	4.5

\*: Beam diameter is defined as intensity decreases to  $1/e^2$  of peak value

\*\*: Resolution is defined as beam diameter at LCM layer

well-aligned pulse shaper. The encoded pulse is broadened to an  $\sim 100$ -ps pseudonoise waveform by spectral phase coding with a length-127 M-sequence (MS) code (a pseudorandom binary phase code with phase shifts of 0 or  $\pi$ ) [35]. 127 pixels are used for the length-127 code, while setting the unused pixel at 0 phase. The 15.6-dB peak intensity contrast ratio between the two traces clearly illustrates the stretching of input short pulses into time-spread noiselike pulses by pseudorandom spectral phase coding. The inset figure shows an encoded pulse with enhanced vertical scale to demonstrate the fine temporal structure present on the encoded waveform. The 8.5-dB fiber-to-fiber insertion loss of this high-resolution shaper is relatively high due to poor coupling back to the large beam size (5.4 mm) collimator, which has to be used to achieve small beam size (high resolution) at the LCM layer. Loss reduction is possible by optimizing the fiber to free-space beam delivery system.

Constructing a low-loss pulse shaper is important for practical application in the OCDMA system. Using a smaller beam size (1.9-mm) collimator, we are able to achieve as low as 4.0-dB fiber-to-fiber insertion loss, which is the lowest value ever reported. The loss is distributed as follows: 2.0 dB from the polarization controller and circulator, 1.0 dB from the LCM, and the remaining 1.0 dB from other components, including collimator input/output coupling, grating diffraction loss, lens and retro-

reflective mirror. Alignment-related loss is included in this latter 1.0 dB. Further loss reduction may require lower loss components (e.g., the circulator). The resolution at the LCM plane is degraded to 300  $\mu\text{m}$  due to the smaller beam size collimator, which supports up to 42 spectral chips because each chip has to be represented by three pixels. Nevertheless, it is sufficient for our system experiment where length-31 codes are used.

In order to form a matched encoder/decoder pair, the spectral coding range covered by the 128 pixels of the LCM has to be identical for both shapers. In addition, due to its programmable nature, the decoder in our experiments can be tuned to decode each of the four users. Consequently, all four pulse shapers (three encoders and one decoder) are carefully constructed to have a nearly identical spectral-phase-coding range. The detailed parameters of these four pulse shapers and the high-resolution pulse shaper discussed previously are listed in Table II. Note that the matched encoder/decoder pair does not necessarily require identical pulse shaper designs, but only requires identical spectral coding range and sufficient resolution. Actually, the designs of the four pulse shapers implemented in our system experiment are considerably different, including diverse selections of collimators, gratings, and lenses. This demonstrates, for the first time to the authors' knowledge, successful implementation of an encoder/decoder pair using different pulse shaper designs.

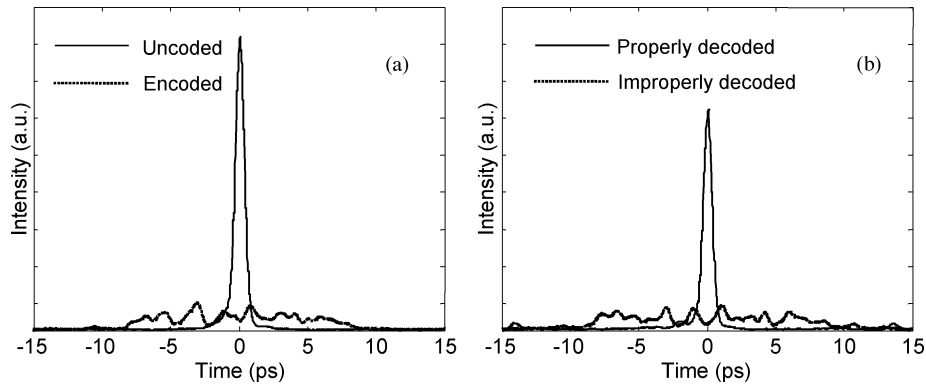


Fig. 9. Intensity cross-correlation measurements. (a) Uncoded (solid line) and 31 MS encoded (dotted line) pulses. (b) Properly decoded (solid line) and improperly decoded (dotted line) pulses.

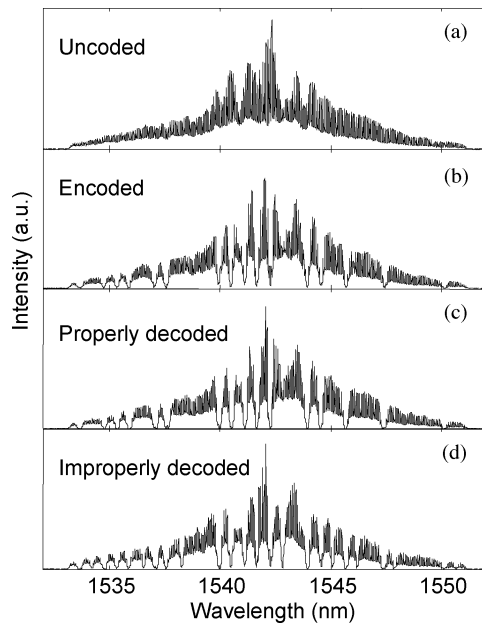


Fig. 10. Optical spectra measurements. (a) Uncoded, (b) 31 MS encoded, and (c) properly decoded and (d) improperly decoded. Optical spectrum analyzer (OSA) resolution: 0.05 nm.

Fig. 9(a) shows intensity cross-correlation measurements of uncoded and encoded  $\sim 20$ -ps pseudonoise waveforms with a length-31 MS code from user 1. It shows behavior similar to Fig. 8 but with less broadening of the pseudonoise waveform because of the smaller number of code chips. Fig. 9(b) shows decoded pulses after two shapers forming an encoder/decoder pair. The improperly decoded pulse remains a broadened pseudonoise waveform as MAI. The properly decoded pulse is converted back to a short pulse with 1.4-dB coding loss and minimal side lobes located at  $\pm 14.3$  ps, which clearly demonstrates successful decoding in the time domain. The properly decoded pulse is slightly broadened to  $\sim 450$  fs due to the coding process and residual dispersion.

Fig. 10 shows optical spectra measurements of uncoded, encoded, and properly and improperly decoded pulses corresponding to the time-domain traces shown in Fig. 9. The spectrum for the uncoded pulse in Fig. 10(a) shows  $\sim 17.9$ -nm spectral coding range cut at the edge of the input spectrum. Clear spectral dips are observed in the encoded/decoded spectra in Fig. 10(b)–(d) whenever a  $0 - \pi$  phase transition occurs

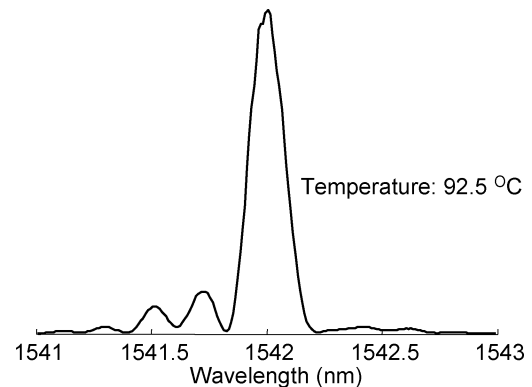


Fig. 11. PPLN waveguide SHG phase-matching spectrum.

in the spectrum explaining the 1.4-dB coding loss, side lobes, and slight pulse broadening mentioned previously. The dips in the spectra are related to diffraction effects arising from the frequency components of the input pulse which fall at  $0 - \pi$  transitions of the LCM in the pulse shaper, which has been quantitatively clarified by simulation and theoretical analysis [15], [42]. The properly decoded pulse spectrum in Fig. 10(c) looks very similar to the encoded one in Fig. 10(b) except for slightly wider spectral dips, since the dips generated by the encoder and decoder are located exactly at the same position, which clearly shows successful decoding in the frequency domain. Finally, there are more dips on the spectrum of the improperly decoded pulse in Fig. 10(d) because  $0 - \pi$  transitions between the encoder and decoder are different.

### C. Nonlinear Processing Based on PPLN

As discussed in the introduction section, a nonlinear optical intensity discriminator plays a critical role in separating properly decoded short pulses from improperly decoded MAI. In our testbed, successful information recovery from MAI is achieved by the use of a novel ultrasensitive nonlinear optical intensity discriminator based on second harmonic generation (SHG) in a PPLN waveguide. The PPLN chip is 67 mm long with 62 mm periodically poled and a channel waveguide fabricated by reverse proton exchange [43]. The propagation losses were 0.2 dB/cm. Fig. 11 shows the PPLN waveguide SHG phase-matching spectrum, which exhibits a  $\text{sinc}^2$ -shape with 0.17-nm bandwidth centered at 1542 nm by temperature tuning to 92.5 °C. Its center wavelength shifts  $\sim 0.1$  nm/°C,

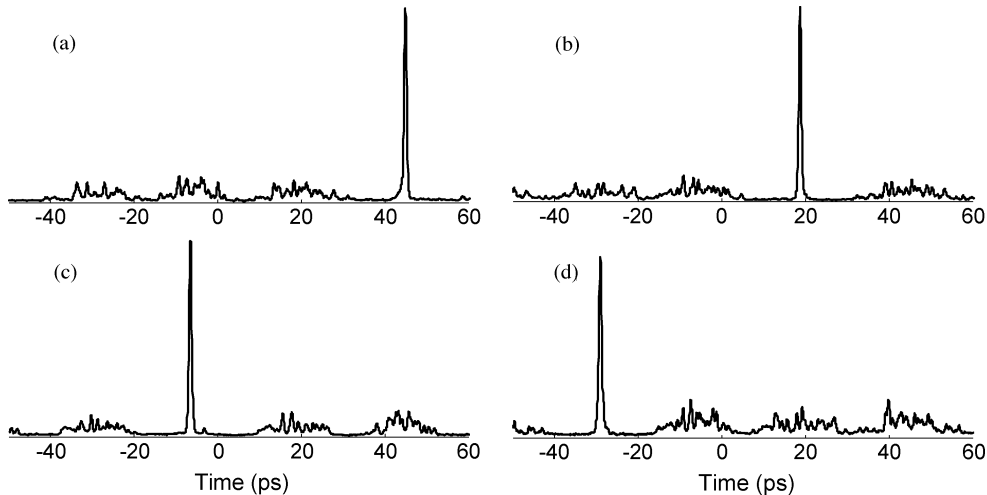


Fig. 12. Intensity cross-correlation measurements of properly decoded channels 1–4 [(a)–(d), respectively] demonstrating the ability to selectively decode any of the four user channels. Channel 4 (d) is the uncoded user.

with almost the same profile. The phase-matching bandwidth is consistent with 18.6-ps temporal walk-off between the fundamental and SHG fields. Asymmetry of the phase-matching curve may be attributed to uneven temperature distribution across the PPLN chip. The measured internal SHG efficiency at the peak of the phase-matching curve is 3100%/W for continuous wave (CW) and 170%/pJ for ultra-short pulses. In the future, even higher efficiency and thus stronger discrimination may be possible by fabricating even longer waveguides.

The use of a waveguide structure together with a long nonlinear medium leads to dramatically increased SHG conversion efficiency for uncoded or properly decoded (bandwidth-limited) pulses [43]; on the other hand, SHG can be strongly suppressed for spectral-phase-encoded or improperly decoded pulses. Roughly speaking, two distinct mechanisms can contribute to suppression of the SHG signal. First, in conventional SHG with large phase-matching bandwidth, the SHG efficiency scales inversely with the pulsewidth. Second, in SHG with large group velocity walk-off, where the device phase-matching bandwidth is much narrower than the input spectrum (as in our experiments), phase modulation on the pulse can also strongly suppress the conversion efficiency. More precisely, one can control the SHG yield by changing the correlation properties of the applied spectral phase code sequences [44], [45]. In this way, the ability to discriminate between uncoded (properly decoded) and encoded (improperly decoded) pulses is greatly enhanced. As a result, second harmonic power contrast ratios of up to 20.1 dB between uncoded and encoded waveforms were observed when coding with a length-31 MS code in experiments at 10 GHz, with less than 1-mW average power (100 fJ per pulse) in the PPLN waveguide [46]. A key point is that the pulse energies required here are approaching two orders of magnitude lower than those required in previous OCDMA decoding experiments based on nonlinear fiber optics.

### III. SYSTEM EXPERIMENTS

In this section, we present the system experiments, which combine all the key components to form an OCDMA testbed as shown in Fig. 5.

#### A. Four-User 2.5-Gb/s Experiment Results

Fig. 12 demonstrates the ability to properly decode any of the four-user channels by the correct selection of decoder spectral phase code—here, a length-31 MS code. The figure shows intensity cross-correlation measurements of the non-data-modulated stream measured at “measurement point  $\alpha$ ” (just before the nonlinear processor) shown in Fig. 5. In our experiment, the pulses from each user are roughly separated by  $\sim 25$  ps for a time-slotted OCDMA scheme. There is no need for precise control of the time offsets. Fig. 12 clearly demonstrates that the properly decoded user is converted back to a short pulse, while the improperly decoded users (MAI) are noiselike temporally broadened waveforms. These noiselike waveforms show distinct fine temporal structure due to the superposition of different spectral phase codes in the encoder and decoder. For example, user 1 and user 2 will see different noiselike waveforms from interference user 3.

The need for a nonlinear pulse discriminator is dramatically illustrated in Fig. 13, where we use a conventional 1.5- $\mu\text{m}$  photodetector optimized for the 2.5-Gb/s data rate to detect the decoder output prior to entering the nonlinear processor. Fig. 13 shows the temporal profile of both properly decoded [(a)—short pulse] and improperly decoded [(b)—temporally broadened] signals, as seen on a sampling scope. Other than the very small amplitude difference due to coding loss in the pulse shaper, there is no noticeable difference between the signals. This clearly illustrates the main issue in OCDMA with ultra-short pulses: properly decoded and improperly decoded waveforms have fundamentally the same energy, which means they produce the same output from a relatively slow electronic detector, even though they can show strong differences in temporal structure and peak intensity on an ultrafast time scale (as shown in Fig. 12). Further, in a system environment, the signals from all users will be superimposed when viewed by a conventional photoreceiver with bandwidth optimized for the data rate. Fig. 13(c) and (d) shows cases of two and four users; the eyes are completely closed. It is very interesting to observe the double and quadruple eyes in (c) and (d). For the two-user case in (c), the double eye can be understood by the following. The top line of the eye corresponds to “1” bits that

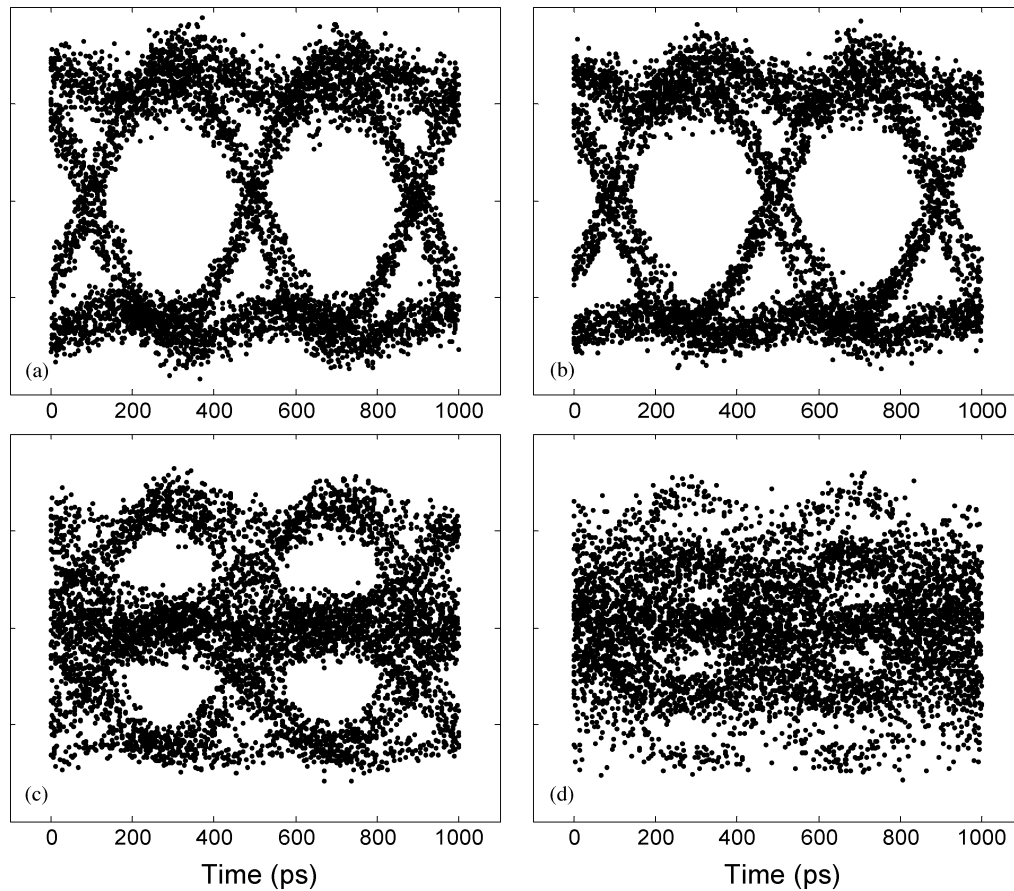


Fig. 13. Eye diagrams prior to nonlinear processing (measurement point  $\alpha$  in Fig. 5). (a) Single-user properly decoded, (b) single-user improperly decoded, (c) two users, and (d) four users. (a) and (b) demonstrate that both properly decoded and improperly decoded single-user channels look essentially identical on a linear detector. (c) and (d) demonstrate that multiple users cannot be adequately separated using linear detection.

are transmitted by both users because the power is doubled. The bottom line of the eye corresponds to “0” bits that are transmitted by both users because the power is blocked by intensity modulation of the data stream. The middle line of the eye corresponds to “1” and “0” bits that are transmitted by either of the two users, while the second user transmits the conjugate state. In addition, since the probability of transmitting a “1” bit or “0” bit by each of the two users is twice that of simultaneously transmitting either “1” bit or “0” bit, there are twice the number of points in the middle line of the eye, resulting in darker middle lines shown in the figure. A similar explanation follows for the (barely visible) quadruple eyes of four users in Fig. 13(d). From another perspective, these figures also confirm that all four users are fully decorrelated by the different fiber delays experienced by each channel. It is also interesting to point out that for a single user, a relatively slow linear electronic detector can be used to correctly detect the signal even if the spectral-phase-code is unknown because both properly and improperly decoded pulses show essentially the same output as shown in Fig. 13(a) and (b). This means that the potential security advantage of OCDMA is not realized in a single-user system employing OOK. However, security can still exist as shown in Fig. 13(c) and (d) in a multiuser environment, which is of practical interest.

Nonlinear processing enables us to separate these temporally overlapped signals, thereby permitting a multiuser system.

Fig. 14(a)–(d) shows, respectively, the output of the receiver (measurement point  $\beta$  in Fig. 5), for a single properly decoded user, a single improperly decoded user, two users (channel 1 properly decoded), and four users (channel 2 properly decoded) at a power in the nonlinear processing element of  $-3$  dBm per user. The clean eye diagrams clearly demonstrate the ability to properly decode the desired channel and separate it from the interference channels.

Fig. 15 shows BER curves for one, two, and four users at 2.5 Gb/s plotted versus the power at the photoreceiver (“measurement point  $\beta$ ”), with either channel 1 or 2 decoded. In all cases, we were able to measure BERs down to less than  $10^{-11}$ . There is a power penalty of roughly 1.5 dB per interfering user (similar for both decoded channels), which we attribute at least in part to the finite interference suppression ratio of the nonlinear discriminator.

Fig. 16 shows the same BER data as in Fig. 15 but replotted against the total power in the nonlinear discriminator (“measurement point  $\alpha$ ”). With perfect interference suppression, the power required at the discriminator should scale proportional to the number of users. The data show almost exactly a 3-dB power increase in going from one to two users, just as expected. An additional  $\sim 4.5$  dB is required in going from two to four users (for  $10^{-11}$  BER). This is  $\sim 1.5$  dB above the 3-dB expected value, which means there is an  $\sim 1.5$ -dB power penalty referenced to the input of the nonlinear discriminator. The key point,

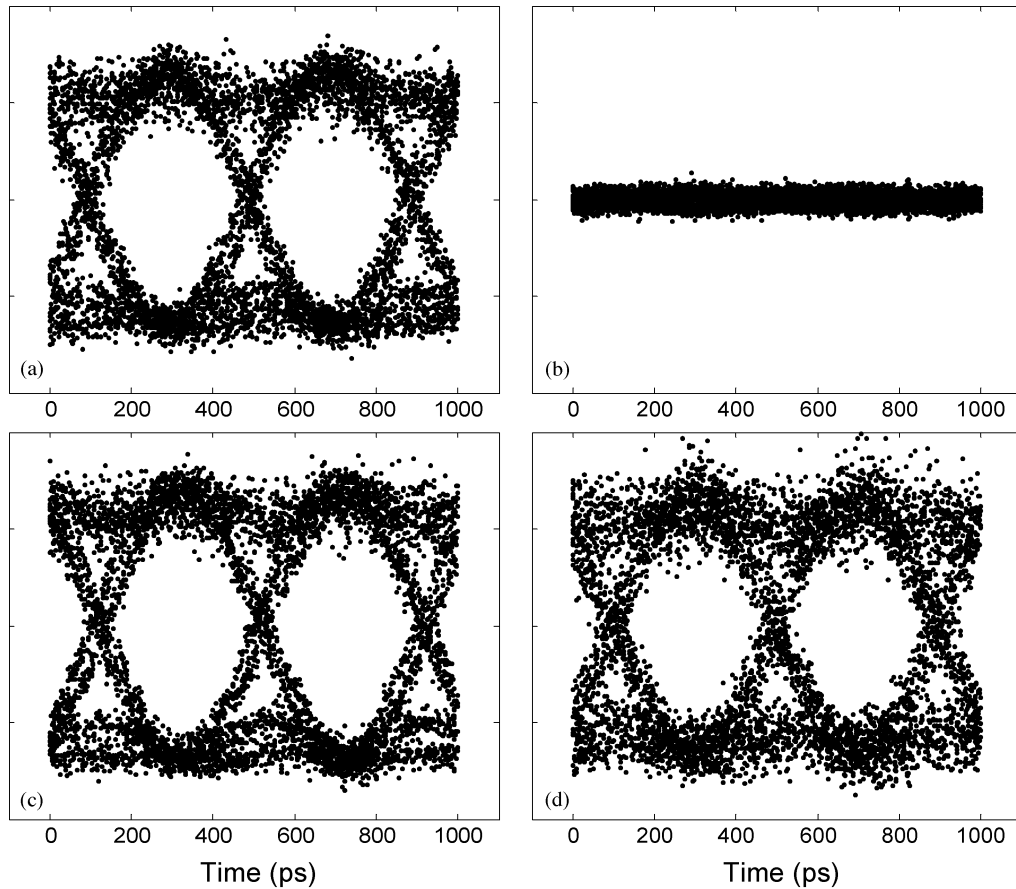


Fig. 14. Eye diagrams after nonlinear processing (measurement point  $\beta$  in Fig. 5) at  $-3$  dBm per user. (a) Properly decoded channel 1, single user. (b) Improperly decoded channel 1, single user. (c) Two-user system, properly decode channel 1. (d) Four-user system, properly decode channel 2. (a) and (b) demonstrate the large contrast between a properly and improperly decoded single-user channel. (c) and (d) demonstrate clear decoding of the desired user in a multiple user system via nonlinear processing.

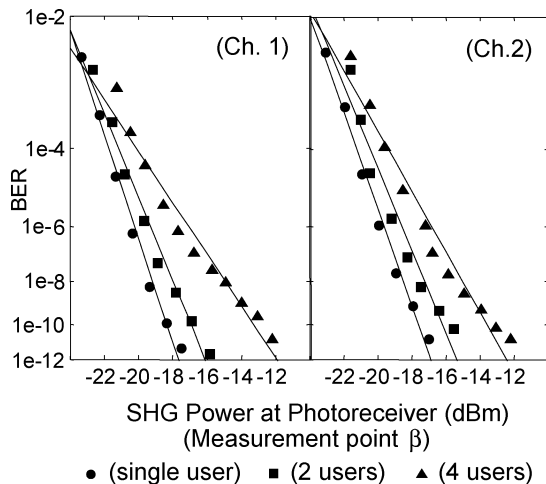


Fig. 15. BER measurements for single user (circles), two users (squares), and four users (triangles). Decoded channel 1 and channel 2 are measured, respectively. Power refers to value at photoreceiver ("measurement point  $\beta$ ").

however, is that we are able to run the four-user experiment at only  $\sim 0.65$  mW per user in the nonlinear element, which provides substantial margin for scaling to higher bit rates and user counts while provisioning only a moderately sized optical amplifier to each receiver node. More precisely, for a single user,

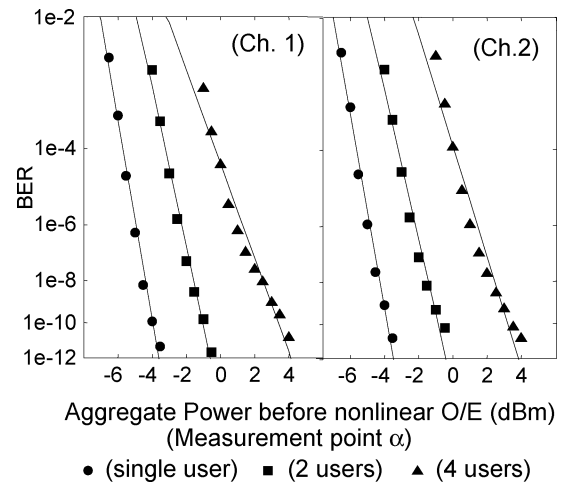


Fig. 16. Same BER data as in Fig. 15 but replotted against the total power in the nonlinear discriminator ("measurement point  $\alpha$ "). BER measurements for single user (circles), two users (squares), and four users (triangles). Decoded channel 1 and channel 2 are measured, respectively.

the required power in the nonlinear element at  $10^{-11}$  BER is  $\sim -3.7$  dBm, which corresponds to an average energy of 171 fJ/b at 2.5 Gb/s. For four users, the required power ( $\sim 4$  dBm) corresponds to an average energy of 251 fJ/b per user.

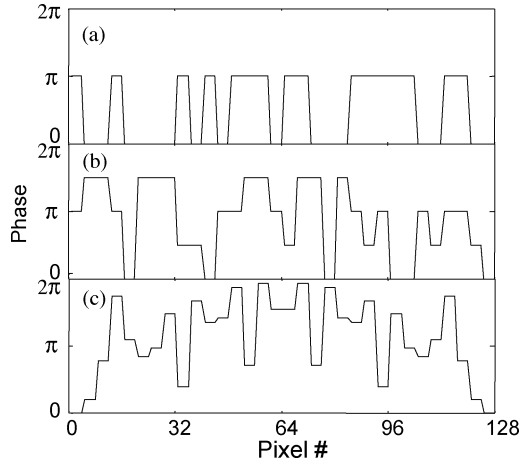


Fig. 17. (a) Length-31 binary (two-level) MS phase codes, (b) quaternary (4-level) phase codes, and (c) quadratic residue (31-level) phase codes.

### B. Multilevel Codes and Capability of Programmable Coding

Our programmable pulse-shaping technique provides flexibility and ease of use in switching to different spectral codes. This could be very helpful in a network environment since code sequence selection plays a critical role in determining the performance of CDMA communication systems [47]. As an example of this capability, in addition to binary MS codes demonstrated in previous sections, we have also applied a four-level (quaternary) family  $\mathcal{A}$  code [47] and a 31-level quadratic residue code [48], as shown in Fig. 17 together with a binary MS code for comparison. Based on the coding literature, multilevel code families can provide a larger number of distinct code sequences with small cross correlation [47]. Figs. 18 and 19 show BER measurements for decoded channel 2, which are obtained by encoding and decoding all users with length-31 quaternary codes and quadratic residue codes, respectively. Note that the aggregate powers before the nonlinear optical-to-electrical (O/E) conversion for two users is somewhat less than 3 dB higher than for one user. Most likely, this occurs because the improperly decoded user experiences higher coding loss than the properly decoded user as illustrated by the greater number of spectral dips shown in Fig. 10; this seems to have a bigger effect in the case of multilevel coding. For four users, the quaternary code shows slightly improved performance to the MS codes, while the quadratic residue code suffers slight degradation. To the authors' knowledge, this is the first demonstration of greater than four-level phase coding in OCDMA systems.

### C. System Degradation Caused by Pulse Overlap Between Users

In our four-user OCDMA demonstration, based on nonlinear processing, there is no need for precise (chip-level) coordination of transmission times or for clock recovery and synchronous gating in the receiver, as discussed in the introduction. However, we have introduced a slot-level coordination scheme and intentionally separated the four users in the time domain, as shown in Fig. 12. We have found that system performance is significantly degraded as pulses overlap between users. Fig. 20 shows the eye diagrams for a two-user experiment while tuning

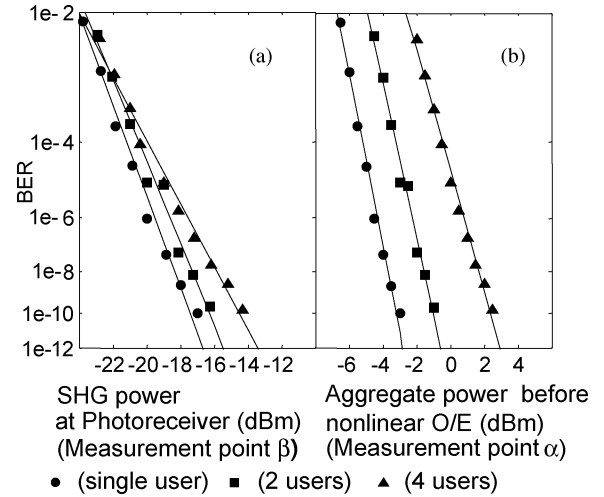


Fig. 18. Decoded channel 2 BER measurements with quaternary codes for single user (circles), two users (squares), and four users (triangles). (a) Power refers to value in nonlinear waveguide ("measurement point  $\alpha$ "). (b) power refers to value at photoreceiver ("measurement point  $\beta$ ").

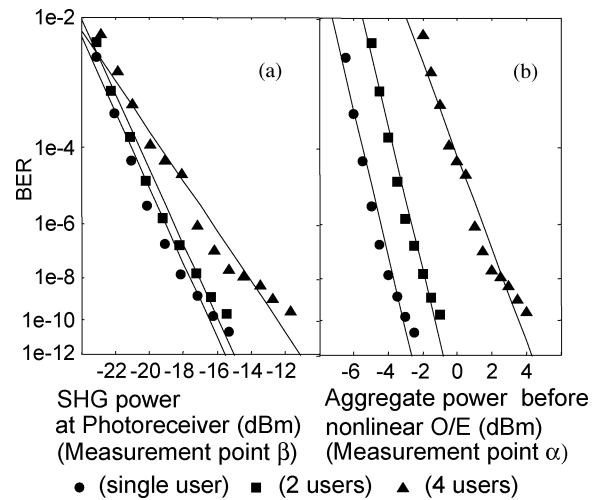


Fig. 19. Decoded channel 2 BER measurements with quadratic residue codes for single user (circles), 2 users (squares), 4 users (triangles). (a) Power refers to value in nonlinear waveguide ("measurement point  $\alpha$ "). (b) Power refers to value at photoreceiver ("measurement point  $\beta$ ").

the pulse separation. When the pulses from the two users are overlapped completely (0-ps separation), the properly decoded user is seriously degraded by the interference channel. The eye becomes clear with increasing temporal separation. The degradation caused by overlapping is almost negligible when the separation is larger than  $\sim 20$  ps. Obviously, such degradation is a kind of beat noise between the signal and interference.

As a qualitative explanation, consider the following example. If the number of chips in the code is  $N = 100$ , the broadened interference waveform intensity is approximately 1% of the short-pulse signal peak intensity. When there is no temporal overlap, the impact of interference is very small after nonlinear processing, since the nonlinear discriminator strongly suppresses the interference signal, and any remaining interference that leaks through the discriminator simply adds (in power) to the desired signal. However, when temporal

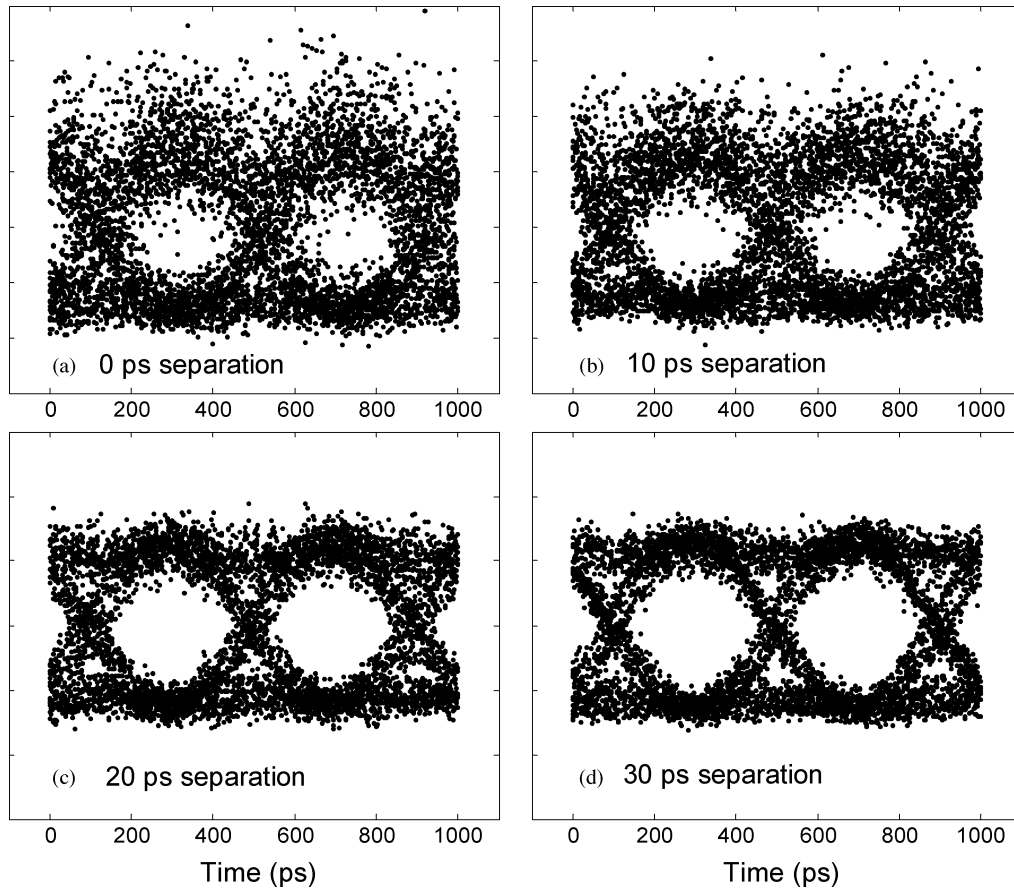


Fig. 20. Degradation caused by pulse overlapping between users. Eye diagrams for two users (channel 1 and 4) with separation (a) 0-ps, (b) 10-ps, (c) 20-ps, and (d) 30-ps separation with decoded channel 1.

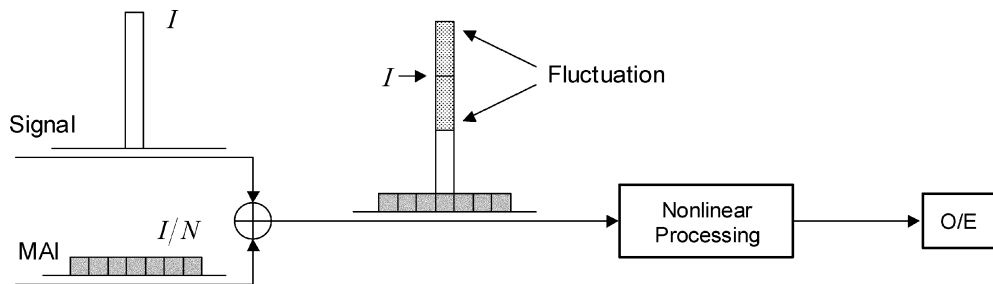


Fig. 21. Illustration of system degradation caused by pulse overlap between users.

overlap occurs, the optical fields (not power) sum at the input of the nonlinear device. For the prior example, the interference-field amplitude is 10% of the signal-field amplitude during the interval of the short pulse. Therefore, the beat-noise intensity fluctuation could be as large as  $\pm 20\%$  (worst case) of the signal intensity (illustrated in Fig. 21). The size of the fluctuation, which is already large, may be increased by the nonlinear optical processing—whether this is performed using an SHG device as was done here, using fiber-based nonlinear optical devices [15], [33], or using other nonlinear devices. The effect of beat noise in ultra-short-pulse OCDMA has been fully analyzed when an ideal thresholder is used at the receiver [10]. However, further analysis is needed when

practical asynchronous nonlinear optical processing devices are placed before the O/E conversion, which of course will depend strongly on the detailed mechanism of the particular nonlinear optical processing device. Degradation caused by overlap is a universal problem for multiuser OCDMA systems [20], [21], [27], [32], [33]. Proposed remedies include optical gating [20], [21], [27] and/or chip-level timing coordination [32], [33]. Optical gating requires clock recovery and a synchronous reference pulse train at the receiver, while chip-level timing coordination requires synchronous control at the transmitter. As a result, both methods sacrifice the advantage of asynchronism. Further investigation into interference suppression methods is needed.

#### IV. DISCUSSION

We have demonstrated a four-user OCDMA system operating at 2.5 Gb/s with a low-power requirement per user, which shows potential for scaling of OCDMA at multigigabit-per-second data rates to significantly higher user counts. However, several factors may affect the practical implementation of an OCDMA system. Some of the issues that would affect practical short-pulse OCDMA operation were discussed in [15], such as splitting loss in a network with broadcast-star architecture and the desirability of miniaturizing the encoder/decoder using integrated devices. One serious problem identified in [15], namely, the requirement of high powers for nonlinear processing, has been addressed in this paper by using a PPLN waveguide operating in a low-power range compatible with current fiber-optic communication systems. Here, we point out some new issues arising from our experiments.

- 1) MAI degradation caused by temporal pulse overlap between users will seriously limit user numbers and complicate control and management for the OCDMA system. In addition to the techniques mentioned previously, we are currently trying to engineer the PPLN design to partially alleviate this effect and improve system performance. In addition, one may use the electrical technique of forward-error correction (FEC) to improve system performance.
- 2) In our current system, we have fiber links consisting of approximately 50 m of SMF and 10 m of DCF. In a network environment, different transmission distances are required, from  $\sim 1$  km for local access and  $\sim 100$  km for metro access. Our group has previously demonstrated distortionless transmission of  $\sim 400$ -fs pulses over a 10-km dispersion-compensated fiber link [49], [50], which may be extendable to an  $\sim 100$ -km range. Although programmable dispersion compensation used in the encoder/decoder allows fine tuning of the overall dispersion balance in the system, each fiber link in the OCDMA system will still need rather precise setting of its fixed-dispersion compensator. Greater precision will be needed if shorter pulses or longer fibers are desired, and this may ultimately limit the usable pulsewidth or fiber span. Polarization-mode dispersion (PMD) will likely also become an issue for scaling transmission of sub-500-fs pulses to the 100-km range.
- 3) The overall capacity in the ideal fully asynchronous ultra-short-pulse OCDMA scheme scales inversely with pulsewidth (for fixed code length) and increases strongly with increased code length (for fixed pulsewidth) [10]. Here, we have demonstrated system operation with 400  $\sim$  500-fs pulses and code length-31 and have performed a fiber-pigtailed pulse-shaping experiment for code length-127. To obtain capacities in the range of  $\sim 100$  Gb/s or above, one needs code lengths in the range of 127 to 511 and shorter pulsewidths (100–300 fs) [10], [15]. Shorter pulsewidths would allow a greater increase in code length, since more spectrum is available for coding. It is possible to achieve  $\sim 100$ -fs high-repetition-rate (10-GHz) pulse trains by soliton compression using dispersion-decreasing fiber followed by pulse cleaning using a nonlinear optical loop mirror (NOLM) [51]. Spectral dispersive devices providing better spectral resolution than diffraction gratings may also contribute to achieving longer code lengths. For example, virtually imaged phased-array (VIPA) spectral dispersers have been demonstrated for spectral coding with 5-GHz resolution [32], and demonstrations of demultiplexing linewidths down to 1.25 GHz [52] show promise for further improvements in pulse-shaper spectral resolution. In addition, substantially longer code lengths would require LCMs (or other modulator array technologies) with more than 128 pixels. LCM devices with 512 [53] and 640 pixels [54] have been previously demonstrated for pulse shaping, and 640-element devices are now commercially available.
- 4) Actively mode-locked fiber lasers are relatively complicated compared with traditional continuous-wave semiconductor lasers used in WDM systems. It may be preferable to utilize high-repetition-rate actively mode-locked lasers based on semiconductor laser technology [55], [56], when these are realized in truly compact form.
- 5) PPLN requires temperature control, which affects the center wavelength of the SHG phase-matching spectrum. The preciseness of temperature control can be relaxed by broadening the phase-matching bandwidth by engineering the PPLN design [57], [58]. In addition, PPLN is polarization sensitive, which may be considered as an advantage in helping suppress MAI because polarizations are randomly distributed among multiple users. However, this also requires polarization control for the desired user, which would complicate receiver design. It is also noted that a polarization-independent device can be realized by methods demonstrated in [59].
- 6) It is worth remarking once more on the relationship between the degree of timing synchronism and performance. In general, increasing timing coordination and synchronism can provide greater user counts and spectral efficiency, at the cost of greater complexity. The analysis of spectral-phase-coded OCDMA in [10] assumed essentially full asynchronism. Improved performance can be expected from the time-slotted scheme investigated here, at a moderate increase in complexity. Further improvement will likely be possible using full chip-level timing coordination in the transmitter and synchronous gating in the receiver with a chip-level timing requirement, at the cost of still greater increase in complexity.

#### V. CONCLUSION

A comprehensive description of an ultra-short-pulse spectral-phase-coded OCDMA system has been presented. On the subsystem level, two key component technologies, namely, femtosecond encoding/decoding and low-power nonlinear discrimination, have been developed and characterized. High-fidelity femtosecond encoding/decoding for length-31 codes has been demonstrated in system experiments. The feasibility of

coding with up to length-127 codes is also demonstrated. High-contrast nonlinear processing using SHG in a PPLN waveguide permits excellent discrimination against MAI while operating at low power, which enables the multiuser OCDMA system to operate at practical power levels compatible with traditional optical communication systems. At the system level, for the first time, a four-user OCDMA system operating at 2.5 Gb/s requiring  $\sim 200$  fJ/b for each user was demonstrated. Multi-level codes have also been demonstrated, which provides the possibility of adding more addresses than would be available for binary codes. Finally, some of the issues and challenges for practical ultrafast OCDMA operation have been discussed.

#### REFERENCES

- [1] A. H. Gnauck *et al.*, "6  $\times$  42.7 Gb/s transmission over ten 200 km EDFA-amplified SSMF spans using polarization-alternating RZ-DPSK," presented at the 2004 Optical Fiber Communication Conf. (OFC'04), Los Angeles, CA, 2004, Postdeadline Paper PDP35.
- [2] G. Charlet *et al.*, "WDM transmission at 6 Tbit/s capacity over transatlantic distance, using 42.7 Gb/s differential phase-shift keying without pulse carver," presented at the 2004 Optical Fiber Communication Conf. (OFC'04), Los Angeles, CA, 2004, Postdeadline Paper PDP36.
- [3] L. Becouarn *et al.*, "42  $\times$  42.7 Gb/s RZ-DPSK transmission over a 4820 km long NZDSF deployed line using C-band-only EDFAs," presented at the 2004 Optical Fiber Communication Conf. (OFC'04), Los Angeles, CA, 2004, Postdeadline Paper PDP37.
- [4] N. Yoshikane *et al.*, "1.14 b/s/Hz spectrally-efficient 50  $\times$  85.4 Gb/s transmission over 300 km using copolarized CS-RZ DQPSK signals," presented at the 2004 Optical Fiber Communication Conf. (OFC'04), Los Angeles, CA, 2004, Postdeadline Paper PDP38.
- [5] J. P. Turkiewicz *et al.*, "Field trial of 160 Gbit/s OTDM add/drop node in a link of 275 km deployed fiber," presented at the 2004 Optical Fiber Communication Conf. (OFC'04), Los Angeles, CA, 2004, Postdeadline paper PDP1.
- [6] T. Ohara, H. Takara, I. Shake, K. Mori, K. Sato, S. Kawanishi, S. Mino, I. Yamada, A. Ishii, I. Ogawa, T. Kitoh, K. Magari, A. Okamoto, R. V. Roussev, J. R. Kurz, K. R. Parameswaran, and M. M. Fejer, "160-Gb/s OTDM transmission using integrated all-optical MUX/DEMUX with all-channel modulation and demultiplexing," *IEEE Photon. Technol. Lett.*, vol. 16, no. 2, pp. 650–652, Feb. 2004.
- [7] J. Shah, "Optical CDMA," *Optics Photonics Newslett.*, vol. 14, pp. 42–47, Apr. 2003.
- [8] D. D. Sampson, G. J. Pendock, and R. A. Griffin, "Photonic code division multiple access communications," *Fiber Integr. Opt.*, vol. 16, pp. 129–157, 1997.
- [9] A. M. Weiner and J. A. Salehi, "Optical code-division multiple access," in *Photonics in Switching*, J. E. Midwinter, Ed. San Diego, CA: Academic, 1993, vol. 2, pp. 73–118.
- [10] J. A. Salehi, A. M. Weiner, and J. P. Heritage, "Coherent ultrashort light pulse code-division multiple access communication systems," *J. Lightw. Technol.*, vol. 8, no. 3, pp. 478–491, Mar. 1990.
- [11] R. Papannareddy and A. M. Weiner, "Performance comparison of coherent ultrashort light pulse and incoherent broad-band CDMA systems," *IEEE Photon. Technol. Lett.*, vol. 11, no. 12, pp. 1683–1685, Dec. 1999.
- [12] P. R. Prucnal, M. A. Santoro, and T. R. Fan, "Spread spectrum fiber-optic local area network using optical processing," *J. Lightw. Technol.*, vol. 4, no. 5, pp. 547–554, May 1986.
- [13] R. A. Griffin, D. D. Sampson, and D. A. Jackson, "Coherence coding for photonic code-division multiple access networks," *J. Lightw. Technol.*, vol. 13, no. 9, pp. 1826–1837, Sep. 1995.
- [14] D. Zaccarin and M. Kavehrad, "An optical CDMA system based on spectral encoding of LED," *IEEE Photon. Technol. Lett.*, vol. 5, no. 4, pp. 479–482, Apr. 1993.
- [15] H. P. Sardesai, C.-C. Chang, and A. M. Weiner, "A femtosecond code division multiple access communication system test-bed," *J. Lightw. Technol.*, vol. 16, no. 11, pp. 1953–1964, Nov. 1998.
- [16] S. Shen, A. M. Weiner, and G. D. Sucha, "Bit error rate performance of ultrashort-pulse optical CDMA detection under multi-access interference," *Electron. Lett.*, vol. 36, pp. 1795–1797, Oct. 2000.
- [17] S. Shen and A. M. Weiner, "Suppression of WDM interference for error-free detection of ultrashort-pulse CDMA signals in a hybrid optical WDM-CDMA system," *IEEE Photon. Technol. Lett.*, vol. 13, no. 1, pp. 82–84, Jan. 2001.
- [18] H. Tsuda, H. Takenouchi, T. Ishii, K. Okamoto, T. Goh, K. Sato, A. Hirano, T. Kurokawa, and C. Amano, "Spectral encoding and decoding of 10 Gbit/s femtosecond pulses using high resolution arrayed-waveguide grating," *Electron. Lett.*, vol. 35, pp. 1186–1188, Jul. 1999.
- [19] N. Wada and K. Kitayama, "A 10 Gb/s optical code division multiplexing using 8-chip optical bipolar code and coherent detection," *J. Lightw. Technol.*, vol. 17, no. 10, pp. 1758–1765, Oct. 1999.
- [20] H. Sotobayashi, W. Chujo, and K. Kitayama, "1.6-b/s/Hz 6.4-Tb/s QPSK-OCDMA/WDM (4 OCDMA  $\times$  40 WDM  $\times$  4 Gb/s) transmission experiment using optical hard thresholding," *IEEE Photon. Technol. Lett.*, vol. 14, no. 4, pp. 555–557, Apr. 2002.
- [21] ———, "Highly spectral-efficient optical code-division multiplexing transmission system," *IEEE J. Sel. Topics Quantum Electron.*, vol. 10, no. 2, pp. 250–258, Mar./Apr. 2004.
- [22] S. Kutsuzawa, N. Minato, S. Oshiba, A. Nishiki, and K. Kitayama, "10 Gb/s,  $\times$  2 ch signal unrepeatable transmission over 100 km of data rate enhanced time-spread/wavelength-hopping OCDM using 2.5-Gb/s-FBG encoder/decoder," *IEEE Photon. Technol. Lett.*, vol. 15, no. 2, pp. 317–319, Feb. 2003.
- [23] M. R. Mokhtar, M. Ibsen, P. C. Teh, and D. J. Richardson, "Reconfigurable multilevel phase-shift keying encoder-decoder for all-optical networks," *IEEE Photon. Technol. Lett.*, vol. 15, no. 3, pp. 431–433, Mar. 2003.
- [24] P. C. Teh, M. Ibsen, and D. J. Richardson, "Demonstration of a full-duplex bidirectional spectrally interleaved OCDMA/DWDM system," *IEEE Photon. Technol. Lett.*, vol. 15, no. 3, pp. 482–484, Mar. 2003.
- [25] J. H. Lee, P. C. Teh, Z. Yusoff, M. Ibsen, W. Belardi, T. M. Monro, and D. J. Richardson, "A holey fiber-based nonlinear thresholding device for optical CDMA receiver performance enhancement," *IEEE Photon. Technol. Lett.*, vol. 14, no. 6, pp. 876–878, Jun. 2002.
- [26] P. C. Teh, M. Ibsen, J. H. Lee, P. Petropoulos, and D. J. Richardson, "Demonstration of a four-channel WDM/OCDMA system using 255-chip 320-Gchip/s quaternary phase coding gratings," *IEEE Photon. Technol. Lett.*, vol. 14, no. 2, pp. 227–229, Feb. 2002.
- [27] P. Petropoulos, N. Wada, P. C. Teh, M. Ibsen, W. Chujo, K. Kitayama, and D. J. Richardson, "Demonstration of a 64-chip OCDMA system using superstructured fiber gratings and time-gating detection," *IEEE Photon. Technol. Lett.*, vol. 13, no. 11, pp. 1239–1241, Nov. 2001.
- [28] A. Grunnet-Jepsen, A. E. Johnson, E. S. Maniloff, T. W. Mossberg, M. J. Munroe, and J. N. Sweetser, "Fiber Bragg grating based spectral encoder/decoder for lightwave CDMA," *Electron. Lett.*, vol. 35, pp. 1096–1097, Jun. 1999.
- [29] ———, "Demonstration of all-fiber sparse lightwave CDMA based on temporal phase encoding," *IEEE Photon. Technol. Lett.*, vol. 11, no. 10, pp. 1283–1285, Oct. 1999.
- [30] D. Gurkan, S. Kumar, A. Sahin, A. Willner, K. Parameswaran, M. Fejer, D. Starodubov, J. Bannister, P. Kamath, and J. Touch, "All-optical wavelength and time 2-D code converter for dynamically-reconfigurable O-CDMA networks using a PPLN waveguide," presented at the 2003 Optical Fiber Communication Conf. (OFC'03), Atlanta, GA, 2003, Paper FD6.
- [31] J. E. McGeehan, S. M. Reza, M. Nezam, P. Saghari, A. E. Willner, R. Omrani, and V. Kumar, "3D time-wavelength-polarization OCDMA coding for increasing the number of users in OCDMA LANs," presented at the 2004 Optical Fiber Communication Conf. (OFC'04), Los Angeles, CA, 2004, Paper FE5.
- [32] S. Etemad, T. Banwell, S. Galli, J. Jackel, R. Menendez, P. Toliver, J. Young, P. Delfyett, C. Price, and T. Turpin, "Optical-CDMA incorporating phase coding of coherent frequency bins: concept, simulation, experiment," presented at the 2004 Optical Fiber Communication Conf. (OFC'04), Los Angeles, CA, 2004, Paper FG 5.
- [33] K. Li, W. Cong, V. J. Hernandez, R. P. Scott, J. Cao, Y. Du, J. P. Heritage, B. H. Kolner, and S. J. B. Yoo, "10 Gbit/s optical CDMA encoder-decoder BER performance using HNLF thresholding," presented at the 2004 Optical Fiber Communication Conf. (OFC'04), Los Angeles, CA, 2004, Paper MF87.
- [34] Z. Jiang, D. S. Seo, S.-D. Yang, D. E. Leaird, A. M. Weiner, R. V. Roussev, C. Langrock, and M. M. Fejer, "Four user, 2.5 Gb/s, spectrally coded O-CDMA system demonstration using low power nonlinear processing," presented at the 2004 Optical Fiber Communication Conf. (OFC'04), Los Angeles, CA, 2004, Paper PDP29.

- [35] R. L. Peterson, R. E. Ziemer, and D. E. Borth, *Introduction to Spread-Spectrum Communications*. Englewood Cliffs, NJ: Prentice-Hall, 1995.
- [36] *Digital Communications*, 1995.
- [37] D. S. Seo, D. E. Leaird, A. M. Weiner, S. Kamei, M. Ishii, A. Sugita, and K. Okamoto, "Continuous 500 GHz pulse train generation by repetition-rate multiplication using arrayed waveguide grating," *Electron. Lett.*, vol. 39, pp. 1138–1140, Jul. 2003.
- [38] A. M. Weiner, J. P. Heritage, and E. M. Kirchner, "High resolution femtosecond pulse shaping," *J. Opt. Soc. Amer.*, vol. B5, pp. 1563–1572, Aug. 1988.
- [39] A. M. Weiner, D. E. Leaird, J. S. Patel, and J. R. Wullert, "Programmable shaping of femtosecond optical pulses by use of a 128-element liquid crystal phase modulator," *IEEE J. Quantum Electron.*, vol. 28, no. 4, pp. 908–920, Apr. 1992.
- [40] A. M. Weiner, "Femtosecond pulse shaping using spatial light modulators," *Rev. Sci. Instrum.*, vol. 71, pp. 1929–1960, May 2000.
- [41] R. Nelson, D. E. Leaird, and A. M. Weiner, "Programmable polarization-independent spectral phase compensation and pulse shaping," *Opt. Exp.*, vol. 11, pp. 1763–1769, Jul. 2003.
- [42] R. N. Thurston, J. P. Heritage, A. M. Weiner, and W. J. Tomlinson, "Analysis of picosecond pulse shape synthesis by spectral masking in a grating pulse compressor," *IEEE J. Quantum Electron.*, vol. QE-22, no. 5, pp. 682–696, May 1986.
- [43] K. R. Parameswaran, R. K. Route, J. R. Kurz, R. V. Roussev, M. M. Fejer, and M. Fujimura, "Highly efficient second-harmonic generation in buried waveguides formed by annealed and reverse proton exchange in periodically poled lithium niobate," *Opt. Lett.*, vol. 27, pp. 179–181, Feb. 2002.
- [44] Z. Zheng and A. M. Weiner, "Spectral phase correlation of coded femtosecond pulses by second-harmonic generation in thick nonlinear crystals," *Opt. Lett.*, vol. 25, pp. 984–986, Jul. 2000.
- [45] Z. Zheng, A. M. Weiner, K. R. Parameswaran, M. H. Chou, and M. M. Fejer, "Low power spectral phase correlator using periodically poled LiNbO<sub>3</sub> waveguides," *IEEE Photon. Technol. Lett.*, vol. 4, no. 4, pp. 376–378, Apr. 2001.
- [46] Z. Jiang, D. S. Seo, S.-D. Yang, D. E. Leaird, A. M. Weiner, R. V. Roussev, C. Langrock, and M. M. Fejer, "Low power, high-contrast coded waveform discrimination at 10 GHz via nonlinear processing," *IEEE Photon. Technol. Lett.*, vol. 16, no. 7, pp. 1778–1780, Jul. 2004.
- [47] S. Boztas, R. Hammons, and P. V. Kumar, "4-phase sequences with near-optimum correlation properties," *IEEE Trans. Inf. Theory*, vol. 38, no. 3, pp. 1101–1113, May 1992.
- [48] M. R. Schroeder, *Number Theory in Science and Communication*. New York: Springer-Verlag, 1985, ch. 15.
- [49] C.-C. Chang, H. P. Sardesai, and A. M. Weiner, "Dispersion-free fiber transmission for femtosecond pulses using a dispersion-compensating fiber and a programmable pulse shaper," *Opt. Lett.*, vol. 23, pp. 283–285, Feb. 1998.
- [50] S. Shen and A. M. Weiner, "Complete dispersion compensation for 400-fs pulse transmission over 10-km fiber link using dispersion compensating fiber and spectral phase equalizer," *IEEE Photon. Technol. Lett.*, vol. 11, pp. 827–829, Jul. 1999.
- [51] K. R. Tamura and M. Nakazawa, "A polarization-maintaining pedestal-free femtosecond pulse compressor incorporating an ultrafast dispersion-imbalanced nonlinear optical loop mirror," *IEEE Photon. Technol. Lett.*, vol. 13, no. 5, pp. 526–528, May 2001.
- [52] S. Xiao, A. M. Weiner, and C. Lin, "Demultiplexers with  $\sim 10$  pm (1.25 GHz) 3 dB transmission bandwidth using virtually imaged phased array," presented at the 2004 Optical Fiber Communication Conf. (OFC'04), Los Angeles, CA, 2004, Paper TuL1.
- [53] H. Wang, Z. Zheng, D. E. Leaird, A. M. Weiner, T. A. Dorschner, J. J. Fijol, L. J. Friedman, H. Q. Nguyen, and L. A. Palmaccio, "20-fs pulse shaping with a 512-element phase-only liquid crystal modulator," *IEEE J. Sel. Topic Quantum Electron.*, vol. 7, no. 4, pp. 718–727, Jul./Aug. 2001.
- [54] G. Stobrawa, M. Hacker, T. Feurer, D. Zeidler, M. Motzkus, and F. Reichel, "A new high-resolution femtosecond pulse shaper," *Appl. Phys. B, Photophys. Laser Chem.*, vol. 72, pp. 627–630, Apr. 2001.
- [55] B. Resan, L. Archundia, P. J. Delfyett, and G. Alphonse, "Dispersion-managed semiconductor mode-locked ring laser," *Opt. Lett.*, vol. 28, pp. 1371–1373, Aug. 2003.
- [56] T. Yilmaz, C. M. DePriest, P. J. Delfyett, S. Etemad, A. Braun, and J. H. Abeles, "Supermode suppression to below -130 dBc/Hz in a 10 GHz harmonically mode-locked external sigma cavity semiconductor laser," *Opt. Exp.*, vol. 11, pp. 1090–1095, May 2003.
- [57] G. Imeshev, M. A. Arbore, M. M. Fejer, A. Galvanauskas, M. Fermann, and D. Harter, "Ultrashort-pulse second-harmonic generation with longitudinally nonuniform quasiphase-matching gratings: pulse compression and shaping," *J. Opt. Soc. Amer. B, Opt. Phys.*, vol. 17, pp. 304–318, Feb. 2000.
- [58] S.-D. Yang, A. M. Weiner, K. R. Parameswaran, and M. M. Fejer, "400-photon-per-pulse ultrashort pulse autocorrelation measurement with aperiodically poled lithium niobate waveguides at 1.55  $\mu\text{m}$ ," *Opt. Lett.*, vol. 29, pp. 2070–2072, Sep. 2004.
- [59] I. Brener, M. H. Chou, E. Chaban, K. R. Parameswaran, M. M. Fejer, S. Kosinski, and D. L. Pruitt, "Polarization-insensitive wavelength converter based on cascaded nonlinearities in LiNbO waveguides," *Electron. Lett.*, vol. 36, pp. 66–67, Jan. 2000.
- [60] R. P. Scott, W. Cong, K. Li, V. J. Hernandez, B. H. Kolner, J. P. Heritage, and S. J. B. Yoo, "Demonstration of an error-free 4  $\times$  10 Gb/s multiuser SPECTS O-CDMA network testbed," *IEEE Photon. Technol. Lett.*, vol. 16, no. 9, pp. 2186–2188, Sep. 2004.
- [61] Z. Jiang, D. S. Seo, D. E. Leaird, A. M. Weiner, R. V. Roussev, C. Langrock, and M. M. Fejer, "Multi-user, 10 Gb/s spectrally phase coded O-CDMA system with hybrid chip and slot-level timing coordination," *IEICE Electron. Express*, vol. 1, pp. 398–403, Oct. 2004.
- [62] Z. Jiang, D. S. Seo, S.-D. Yang, D. E. Leaird, A. M. Weiner, R. V. Roussev, C. Langrock, and M. M. Fejer, "Spectrally coded O-CDMA system with four users at 2.5 Gbit/s using low power nonlinear processing," *Electron. Lett.*, vol. 40, pp. 623–625, May 2004.



fiber nonlinearity.

**Z. Jiang** (S'03) received the B.S. (highest honors) and M.S. degrees from the Department of Electronics Engineering, Tsinghua University, Beijing, China, in 1999 and 2002, respectively. He is currently working toward the Ph.D. degree at the School of Electrical and Computer Engineering, Purdue University, West Lafayette, IN.

He has been author or coauthor of more than 20 journal and conference papers. His research focuses on the areas of ultrafast technology, optical pulse shaping, optical fiber communication, and



**D. S. Seo** (M'00) received the B.S. and M.S. degrees in electronic engineering from Yonsei University, Seoul, Korea, in 1980 and 1985, respectively, and the Ph.D. degree in electrical engineering (optoelectronics) from the University of New Mexico, Albuquerque, in 1989.

He was with the Agency for Defense Development as a Research Engineer from 1980 to 1986. From 1986 to 1990, he was a Research Assistant and later a Research Staff Member at the Center for High Technology Materials, the University of

New Mexico. In 1990, he joined the faculty of Myongji University, Yongin, Korea, where he is currently a Professor in the Department of Electronics. From 1994 to 1995, he was a Visiting Research Fellow at the Photonics Research Laboratory, University of Melbourne, Melbourne, Australia, and from 2002 to 2004, he was with Purdue University, West Lafayette, IN, as a Visiting Research Professor in the School of Electrical and Computer Engineering. His current research interests are in the areas of ultrashort optical pulse sources, very-high-speed optical data generation and transmission, semiconductor lasers, microwave photonics, and optical code-division multiple access.



**S.-D. Yang** (S'01) was born in Chiayi, Taiwan, R.O.C., in April 1975. He received the B.S. degree in electrical engineering from National Tsing-Hua University, Hsinchu, Taiwan, R.O.C., in 1997 and the M.S. degree in electrooptical engineering from National Taiwan University, Taipei, Taiwan, R.O.C., in 1999. He is currently working toward the Ph.D. degree in electrical and computer engineering at Purdue University, West Lafayette, IN, where he is working on ultrafast nonlinear optics and signal processing.



**D. E. Leaird** (M'01) was born in Muncie, IN, in 1964. He received the B.S. degree in physics from Ball State University, Muncie, IN, in 1987 and the M.S. and Ph.D. degrees from the School of Electrical and Computer Engineering, Purdue University, West Lafayette, IN, in 1996 and 2000, respectively.

He joined Bell Communications Research (Bellcore), Red Bank, NJ, as a Senior Staff Technologist in 1987 and later advanced to Member of Technical Staff. From 1987 to 1994, he worked in the Ultrafast Optics and Optical Signal Processing Research

Group, where he was a key team member in research projects in ultrafast optics, such as shaping of short optical pulses using liquid-crystal modulator arrays, investigation of dark soliton propagation in optical fibers, impulsive stimulated Raman scattering in molecular crystals, and all-optical switching. He is currently a Senior Research Scientist and Laboratory Manager of the Ultrafast Optics and Optical Fiber Communications Laboratory in the School of Electrical and Computer Engineering, Purdue University, where he has been since 1994. He has coauthored approximately 55 journal papers and 75 conference proceedings and has one issued U.S. patent and has a second application pending.

Dr. Leaird is active in the optics community and professional organizations, including the Optical Society of America (OSA) and the IEEE Lasers & Electro-Optics Society (LEOS), where he is a Member of the Ultrafast Technical Committee and serves as a consultant to venture capitalists by performing technical due diligence. He also serves as a frequent reviewer for *Optics Letters*, the IEEE PHOTONICS TECHNOLOGY LETTERS, *Applied Optics*, and the *Journal of the Optical Society of America B*. He also serves on National Science Foundation review panels in the SBIR program. He has received several awards for his work in the ultrafast optics field, including a Bellcore Award of Excellence, a Magoon Award for outstanding teaching, and an OSA/New Focus Student Award.



**R. V. Roussev** received the M.Sc. degree in engineering physics (specializing in quantum electronics) from Sofia University, Bulgaria, in 1996 with a thesis in the field of nonlinear optics and photorefractive solitons. He is currently working toward the Ph.D. degree in applied physics at Stanford University, Stanford, CA.

He was a Research Assistant in the Atomic Spectroscopy group at the Bulgarian Academy of Sciences from 1998 to 1999, investigating transition probabilities and radiation lifetimes of excited states of Hg.

His current research interests focus on developing efficient optical frequency conversion in periodically poled lithium niobate (bulk and waveguides) with increased resistance to photorefractive damage.



**C. Langrock** (S'01) received the Diploma degree in physics from Heinrich-Heine-Universität, Düsseldorf, Germany, in 2001. He is currently working toward the Ph.D. degree in electrical engineering at Stanford University, Stanford, CA.

He is also currently a Research Assistant in the Ginzton Laboratory at Stanford University. His research interests include single-photon generation and detection, detection of weak ultrashort optical pulses, and nonlinear optics.

**M. M. Fejer**, photograph and biography not available at the time of publication.



**A. M. Weiner** (S'84-M'84-SM'91-F'95) received the Sc.D. degree in electrical engineering from the Massachusetts Institute of Technology (MIT), Cambridge, in 1984.

He was a Fannie and John Hertz Foundation Graduate Fellow at MIT from 1979 through 1984. In 1984, he joined Bellcore, where in 1989, he was promoted to manager of Ultrafast Optics and Optical Signal Processing. He joined Purdue University, West Lafayette, IN, in 1992 as Professor of Electrical and Computer Engineering. From 1997 to 2003, he

served as Electrical and Computer Engineering (ECE) Director of Graduate Admissions. He is currently the Scifres Distinguished Professor of ECE. His research focuses on ultrafast optical signal processing and high-speed optical communications. He is especially well known for pioneering the field of femtosecond pulse shaping, which enables generation of nearly arbitrary ultrafast optical waveforms according to user specification. He has published four book chapters and more than 130 journal papers. He has been author or coauthor of more than 250 conference papers, including approximately 60 conference invited talks, and has presented more than 70 additional invited seminars at universities or industry. He is holder of six U.S. patents.

Prof. Weiner is a Fellow of the Optical Society of America (OSA). He has received numerous awards for his research, including the Hertz Foundation Doctoral Thesis Prize (1984); the Adolph Lomb Medal of the OSA (1990), awarded for pioneering contributions to the field of optics made before the age of 30; the Curtis McGraw Research Award of the American Society of Engineering Education (1997); the International Commission on Optics Prize (1997); the IEEE Lasers & Electro-Optics Society (LEOS) William Streifer Scientific Achievement Award (1999); the Alexander von Humboldt Foundation Research Award (2000); and the inaugural Research Excellence Award from the Schools of Engineering at Purdue (2003). He has served on or chaired numerous research review panels, professional society award committees, and conference program committees. In 1988–1989, he served as an IEEE LEOS Distinguished Lecturer. He was General Co-Chair of the 1998 Conference on Lasers and Electro-Optics, Chair of the 1999 Gordon Conference on Nonlinear Optics and Lasers, and Program Co-Chair of the 2002 International Conference on Ultrafast Phenomena. In addition, he was Associate Editor for the IEEE JOURNAL OF QUANTUM ELECTRONICS, the IEEE PHOTONICS TECHNOLOGY LETTERS, and *Optics Letters*. He was an elected Member of the Board of Governors of IEEE LEOS from 1997 to 1999 and Secretary/Treasurer of IEEE LEOS from 2000 to 2002. He is currently a Vice-President (representing IEEE LEOS) of the International Commission on Optics (ICO).